ARTICLE

A Simple Route to Highly Oriented and Ordered Nanoporous Block Copolymer Templates

Soojin Park, Jia-Yu Wang, Bokyung Kim, Ji Xu, and Thomas P. Russell*

Department of Polymer Science and Engineering, University of Massachusetts, Amherst, 01003

ABSTRACT Controlling the orientation and lateral ordering of the block copolymer microdomains is essential to their use as templates and scaffolds for the fabrication of nanostructured materials. In addition, a process must be robust, simple to implement, and rapid, and should not introduce disruptive processing steps that would impede their use. Here, we describe thin films of poly(styrene-b-4-vinylpyridine) (PS-b-P4VP) diblock copolymers, spin-coated from mixed solvents that show highly oriented, cylindrical microdomains with a high degree of order on a wide range of substrates, including silicon oxide, polystyrene, germanium, polyimide, and poly(butylene terephthalate). In addition, the preferential solvation of the P4VP block with an alcohol caused a surface reconstruction that resulted in the formation of a nanoporous film upon drying. The evaporation of gold onto the reconstructed films produced thermally stable and reactive ion etching resistant films.

KEYWORDS: PS-b-P4VP · surface reconstruction · block copolymer · perpendicular orientation · gold evaporation · reactive ion etching

Block copolymers, self-assemble into arrays of nanometer-sized domains, making them attractive candidates for the generation of high-density media which is used for data storage,[1] electronics,[2] and molecular separation.[3] Block copolymers have gained increasing attention as templates and scaffolds for the fabrication of high-density arrays of nanoscopic elements because of the size and tunability of the microdomains, the ease of processing on flat and patterned surfaces without introducing disruptive technologies, and the ability to manipulate their functionality.[4–8] For block copolymers having cylindrical microdomains, it is necessary to control the orientation and lateral ordering of the microdomains to optimize the contrast in transfer applications and the density of elements. In addition, it is highly desirable that the process is independent of the underlying substrate. Approaches to control the orientation of the microdomains of block copolymers include the use of solvent fields,[9–12] electric fields,[13] chemically patterned substrates,[14,15] graphoepitaxy,[16] epitaxial crystallization,[17] controlled interfacial interactions,[18,19] thermal gradients,[20] zone casting,[21] and shear.[22]

By removal of the minor component forming the cylindrical microdomains a nanoporous template is produced where the aspect ratio of the pores is dictated by film thickness. While one can rely on this aspect ratio to provide a natural etching contrast, other attempts have been made to enhance the contrast. A common feature of these approaches is to use a block copolymer where one block contains an inorganic element, like Si or Fe, or to load one of the phases with an etch-resistant inorganic component.[23–27] Park *et al.* for example, used an OsO_4-stained microphase-separated thin film of poly(styrene-b-butadiene), which has a reactive ion etch (RIE) contrast of 2:1, and produced an array of holes in the underlying silicon nitride substrates.[6] Spatz *et al.* quarternized poly(styrene-*b*-2-vinylpyridine) (PS-*b*-P2VP) with auric acid, and then deposited gold in the P2VP microdomain, to generate masks for nanolithography.[28] Alternatively, Ti was grown on top of the PS matrix to yield sufficient contrast.[29]

Here, we report that highly oriented cylindrical microdomains with a long-range lateral order in poly(styrene-*b*-4-vinylpyridine) (PS-*b*-P4VP) copolymers thin films are achieved by spin coating the copolymer from a mixed solvent (toluene/THF). As shown in Scheme 1, cylindrical microdomains normal to the surface are obtained directly after spin coating, and this process is independent of underlying substrate. By annealing these films by solvent, arrays of cylindrical microdomains with a high degree of lateral order can be achieved with little change of the interdomain distance. After dipping the films into a preferential solvent for P4VP, which is ethanol in

*Address correspondence to russell@mail.pse.umass.edu.

Received for review December 21, 2007 and accepted March 13, 2008.

Published online April 22, 2008.
10.1021/nn7004415 CCC: $40.75

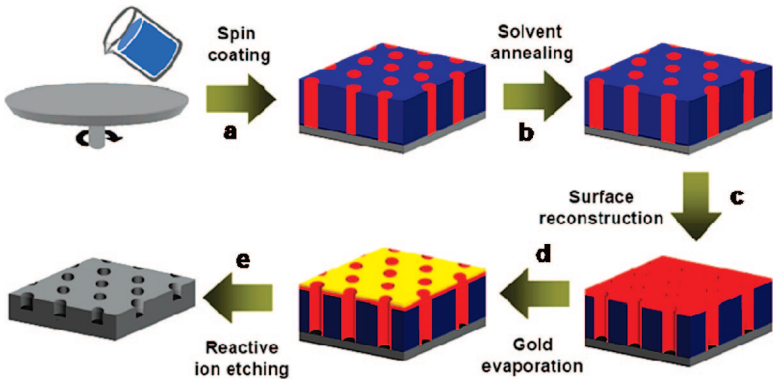

Scheme 1. Schematic representation of the fabrication of nanoporous templates: (a) spin-coating of PS-b-P4VP on a variety of substrates; (b) preparation of highly long-range ordered films *via* solvent annealing; (c) surface reconstruction of ordered films; (d) gold evaporation of the reconstructed films; (e) fabrication of nanoporous templates *via* reactive ion etching.

this work, a nanoporous film can be produced by a fully reversible reconstruction process that leaves P4VP on the surface. Details of the experiment and phase behaviors of PS-b-P4VP films in a toluene/THF solvent mixture were reported previously.[30]

Evaporation of Au (which interacts strongly with P4VP) on the surface of the film at a glancing angle leaves a nanoporous Au film that is ideal for RIE with high-etch contrast for transfer of the pattern to the underlying substrate. The results described here are obtained by solvents and simple fabrication steps that are cost-effective and fully compatible with current industrial processes.

RESULTS AND DISCUSSION

High molecular weight PS-b-P4VP with number average molecular weights of PS and P4VP blocks were 47.6 and 20.9 kDa (kilo Dalton), respectively, and a total polydispersity of 1.14 was used. Figure 1 shows scanning force microscopic (SFM) images of as-spun, solvent-annealed, and surface-reconstructed PS-b-P4VP films on a native silicon substrate. The SFM image of the as-spun film (Figure 1a) shows a surface covered with circular domains, having an average separation distance of 48.4 ± 9.2 nm and an average diameter of 29.6 ± 5.9 nm (see Supporting Information, Figure S1a). These results suggest that the cylindrical microdomains of the P4VP are oriented normal to the surface. Independent TEM measurements (see Supporting Information, Figure S2) of the as-spun film, stained with iodine, confirm that the P4VP microdomains are oriented normal to the film surface. For TEM measurements, the PS-b-P4VP film was floated off the silicon substrate in a 5 wt % HF solution and colleted on a carbon-coated grid (see Supporting Information, Figure S2a).

A hexagonal order of the as-spun films is only in a short-range, which is represented in the Voronoi diagram in Figure 1b.[31] The cylindrical microdomains having six nearest neighbors are not colored, and those with four, five, seven, and eight nearest neighbors are marked in blue, red, green, and pink, respectively. There are many defects in the Voronoi diagram in the case of as-spun films as shown in Figure 1b. After the as-spun films were exposed to the toluene/THF mixtures under nitrogen at room temperature for 6 h, a hexagonal array of the circular domains with a significantly enhanced lateral order was obtained (Figure 1c). Figure 1d shows a perfect hexagonal order as

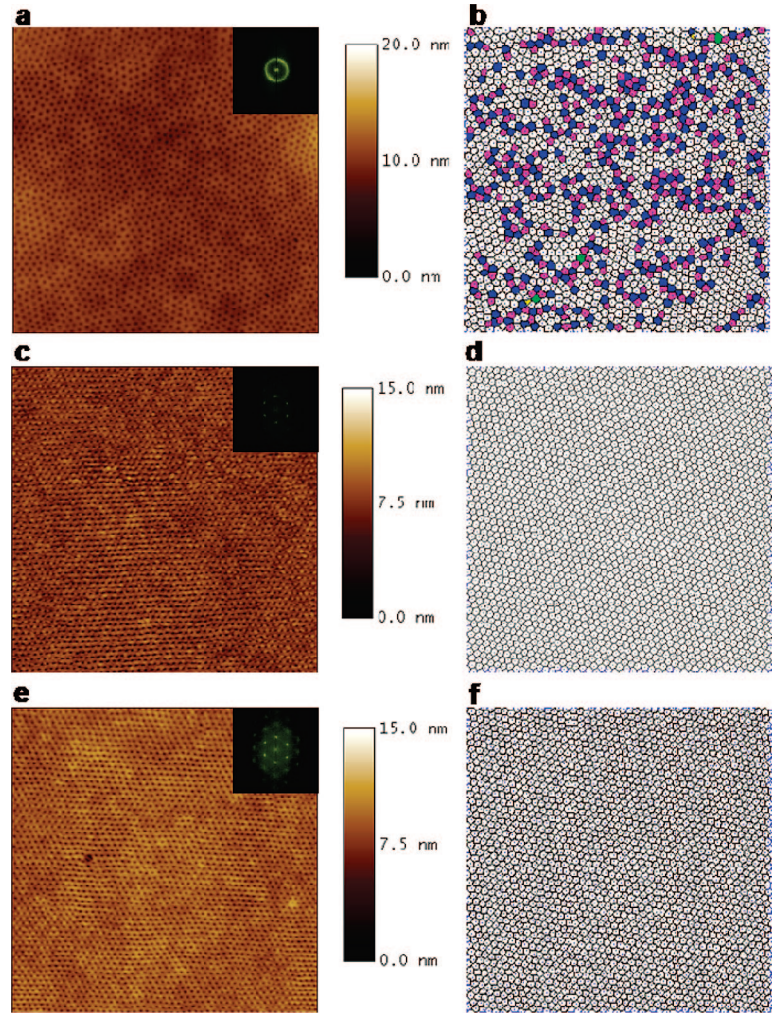

Figure 1. SFM images of highly ordered PS-b-P4VP films to silicon substrates (2 μm × 2 μm size, height mode): (a) as-spun films; (c) well-developed hexagonal structure *via* solvent annealing; (e) surface reconstruction of the ordered films. Fourier transform of panels c and e show the characteristic of the long-range order in the inset. Voronoi diagrams (b, d, and f) constructed from domain center locations show the population of point defects.

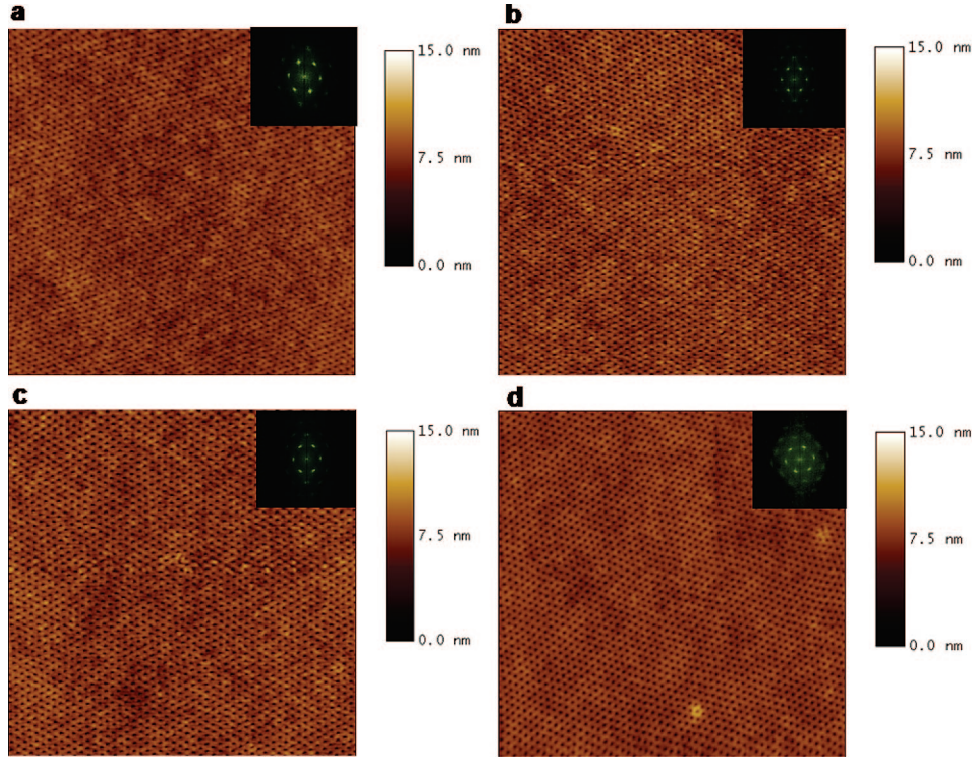

Figure 2. SFM images of surface reconstructed PS-b-P4VP films on a variety of substrates (2 μm × 2 μm size, height mode): (a) polystyrene, (b) germanium, (c) polyimide, (d) poly(butylene terephthalate). The impressive degree of order is reflected in the Fourier transform as shown in the inset.

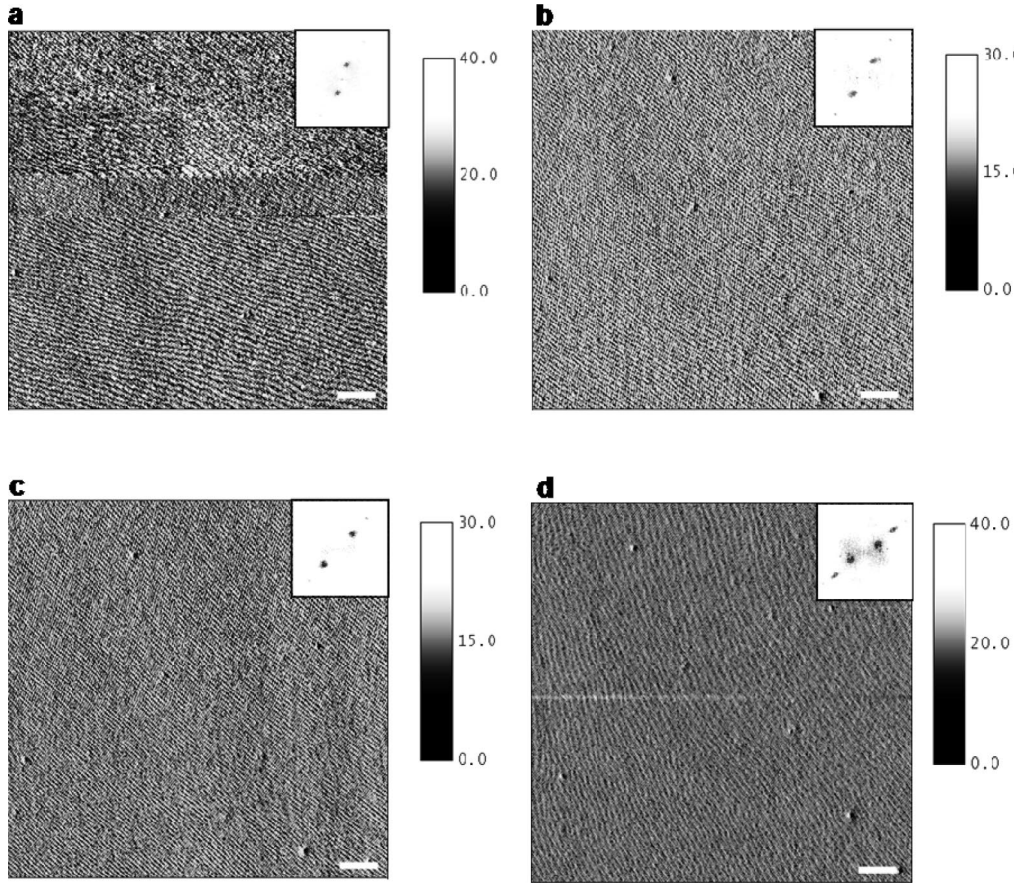

Figure 3. Moiré patterns of highly ordered PS-b-P4VP films measured from SFM at four different scan angles (scale bar: 1 μm): (a) scan angle, 0°; (b) scan angle, 5°; (c) scan angle, 10°; and (d) scan angle, 20°. These results show the large grain size and uniaxial direction of PS-b-P4VP cylindrical microdomains.

shown in the Voronoi diagram. Independent TEM measurements confirmed that the cylindrical microdomains were oriented normal to the film surface. When the well-developed films were immerged in ethanol, a good solvent for P4VP and a nonsolvent for PS, a reconstruction of the film was observed with a highly ordered array of nanoscopic pores (Figure 1e). The surface reconstruction of the film keeps well-developed microdomain structure of solvent annealed films, which also having the perfect hexagonal order as shown in the Voronoi diagram of Figure 1f. Here, P4VP block is solubilized by ethanol and, upon drying, the P4VP rests on top of the PS matrix, leaving pores at the positions of the cylindrical P4VP microdomains. This is similar to the result of surface reconstruction of PS-b-PMMA by acetic acid, a preferential solvent for PMMA.[8] Independent X-ray photoelectron spectroscopy (XPS) measurements showed the presence only of P4VP on the surface with no trace of PS. The TEM image of reconstructed films (see Supporting Information, Figure S2b) confirmed the nanoporous structure of the PS-b-P4VP (as schematized in Scheme 1). The film thickness of as-spun and reconstructed PS-b-P4VP samples were found to be 24 and 27 nm, respectively, by X-ray reflectivity (see Supporting Information, Figure S3). When we increased the film thickness up to 60 nm, well-developed cylindrical microdomains oriented normal to the surface could be generated (not shown here). The solvent annealed and reconstructed PS-b-P4VP films are characterized by a hexagonal array of cylindrical microdomains or nanopores with an average nearest-neighbor distance of 45.3 $\pm$ 2.3 nm and pore diameter of 25.0 $\pm$ 1.7 nm (see Supporting Information, Figure S1). The Fourier transforms of the SFM images are shown in the insets of Figure 1c,e, where six-point patterns, with multiple higher-order reflections, are seen, which is characteristic of the long-range order. This process for preparation of nanoporous templates from PS-b-P4VP is general for a wide range of substrates including polystyrene, germanium, polyimide, and poly(butylene terephthalate) as shown in Figure 2.

To characterize the orientation, grain size, and dislocation of cylindrical microdomains, Moiré pattern analyses have been used.[32,33] Moiré patterns are formed from interference between a reference and a sample grating. Under certain conditions, we can observe the grain size, shape, orientation, and dislocation directly. Figure 3 shows Moiré patterns of highly ordered PS-b-P4VP films measured from SFM at four different scan angles. These results show the large single grain size of 10 μm, the uniaxial direction of PS-b-P4VP cylindrical microdomains, and a few dislocation points are shown in Figure 3d.

As another characterization method, we used orientational correlation function to calculate quantitatively the orientational order of solvent annealed PS-b-P4VP films in Figure 1b. The orientational correlation function is defined as[31]

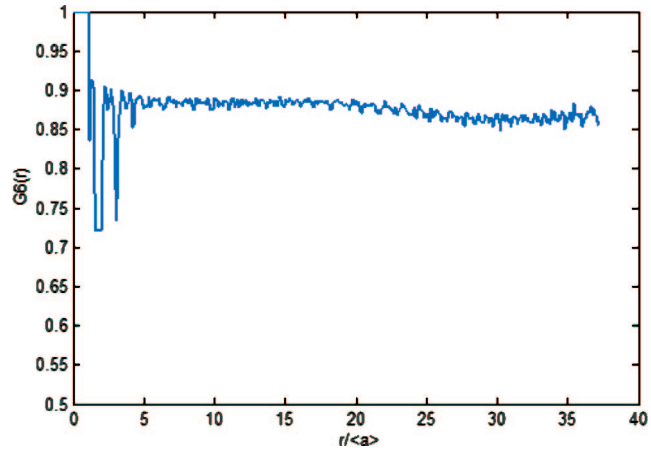

Figure 4. Representative orientational correlation function ($G_6(r)$) calculated from solvent annealed PS-b-P4VP sample ($G_6(r)$ *vs* distance normalized by average interdomain spacing (a). This result shows very little decay even at large area ($r > 35a$), which indicates the presence of long-range orientational order.

$$G_6(r) = \langle \phi_6^*(0)\phi_6(r) \rangle \quad (1)$$

where

$$\phi_6(r_j) = \frac{\sum_{j=1}^{NN} \exp(6i\theta(r_{ij}))}{NN} \quad (2)$$

and $\phi_6^*(0)$ indicates the complex conjugate of the order parameter of the cylindrical microdomains which is designated as the origin, index j counts the nearest-neighbors, NN, of cylinder i, and $\theta(r_{ij})$ is the angle made between the bond connecting cylinders i and j and an arbitrarily chosen reference axis. Each cylinder is used as the origin for one calculation, and the angular brackets indicate an average over all cylinders. $G_6(r)$ has a value between 0 and 1 for all r. For a perfect hexagonal crystal, a plot of $G_6(r)$ *vs* r will have a value of 1 and will only exist when $r = na$, where n has a integer value. In a real crystal, the maximum value of this graph will not be 1.0 because of fluctuations in lattice positions even for a well-ordered 2-D crystal.

Figure 4 shows the orientational correlation function calculated from an SFM image of solvent annealed PS-b-P4VP in Figure 1b. The local bond orientational order is 0.91, which is extremely close to 1, the value of a perfect lattice. $G_6(r)$ decays very little over large distances, which implies the presence of long-range orientational order.

A thin layer of gold was evaporated onto the surface of the reconstructed films by orienting the film surface at an angle of ~5° with respect to the path of the gold atoms from the target in the evaporator. This prevented the evaporation of gold on the walls of the

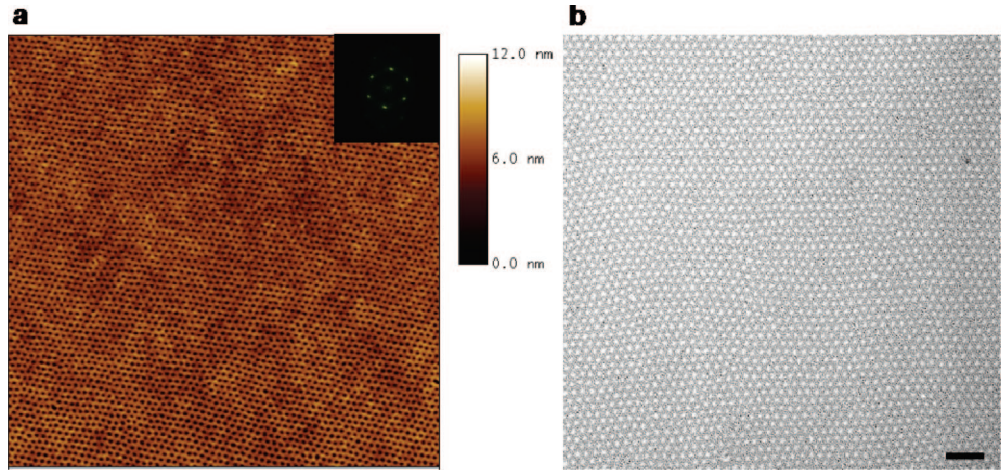

Figure 5. SFM and TEM images of highly ordered PS-b-P4VP films with small molecular weight. SFM image of surface reconstructed films (2 μm × 2 μm size, height mode): (a) TEM image of Au evaporated films after surface reconstruction (scale bar: 100 nm); (b) the Fourier transform of Figure 3a shows the impressive degree of order as well those of high-molecular-weight PS-b-P4VP.

pores in the films.[34] The thickness of gold layer was ~0.7 nm, as determined by X-ray reflectivity (see Supporting Information, Figure S3). The gold layer on the surface of the film was investigated using grazing incidence small-angle X-ray scattering (GISAXS). GISAXS measurements were performed on the X22B beamline (National Synchrotron Light Source, Brookhaven National Laboratory) using X-ray with a wavelength of λ = 1.525 Å (see Supporting Information, Figure S4). These results confirmed the existence of a ~1 nm thick gold layer on the reconstructed films that had pores located at the positions of the original pores in the films and that the gold was kept to the surface of the film without coating the pore walls. Measurements performed as a function of temperature indicated that for films without the gold on the surface the nanoporous structure was lost at ~115 °C, while with gold on the surface, the nanoporous structure was retained up 200 °C. Consequently, the presence of the gold retarded the flow of the PVP back in to the nanopores in the PS matrix.

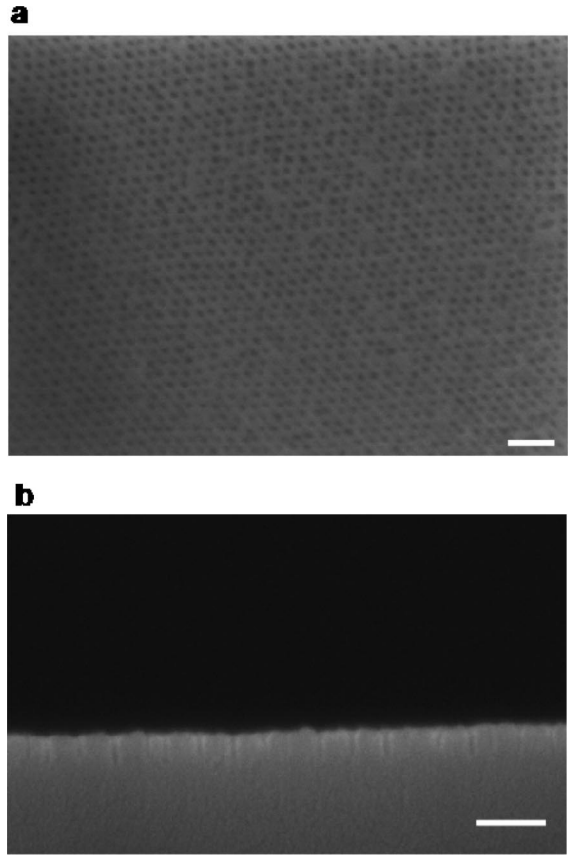

Figure 6. SEM images of highly ordered nanoporous templates fabricated on the silicon substrate *via* reactive ion etching (scale bar: 100 nm): top view (a) and cross-sectional view (b) were shown.

Experiments were also performed on PS-b-P4VP where the molecular weights of the PS and P4VP blocks were 25.0 and 7.0 kDa, respectively, with M_w/M_n = 1.09 (purchased from Polymer Source). Figure 5 shows SFM and TEM images of PS-b-P4VP after spin coating and solvent annealing with a toluene/THF mixture, followed by swelling with alcohol and drying, to produce a nanoporous template. The film thickness of solvent annealed and reconstructed PS-b-P4VP samples were found to be 20 and 22.5 nm, respectively, by ellipsometry. The Fourier transform of Figure 5a is shown in the inset, where a six-point pattern, with multiple higher-order reflections, is obtained, characteristic of the long-range lateral order. Subsequently, a ~1 nm thick layer of gold was evaporated onto the surface of the films at a glancing angle, which yielded the TEM image in Figure 5b. Here, a hexagonal array of 15.2 ± 1.3 nm diameter pores and center-to-center distance of 25.1 ± 1.2 nm in the gold film is seen (see Supporting Information, Figure S5). A lower magnification SEM image (see Supporting Information, Figure S6) showed that the lateral order persisted over and area of 3 × 2 μm^2 scale in the low magnification TEM, though independent measure-

ments showed that such structures could be achieved at a 10 × 10 μm^2 area. The gold-coated films were exposed to a CF_4 RIE at 65 W for 40 s.[35] After etching the silicon oxide, gold-coated films were removed with a 10 wt % KI/I_2 (4/1, v/v) solution followed by heating to 400 °C for 3 h.

Figure 6 shows SEM images of an array of holes that were etched into the underlying silicon oxide, which are identical to that seen in the original template. The top view (Figure 6a) indicates a highly ordered nanoporous structures with areal density of $\sim 10^{11}/cm^2$ holes, while the cross-sectional view (Figure 6b) shows etching depth with a high aspect ratio of ~3:1. It should be noted that the fidelity of the transfer could not be achieved without the use of the gold layer to enhance the etching contrast. In addition, alternative lift-off procedures by chloroform could be used as effectively.

CONCLUSIONS

In conclusion, we have shown that using a combination of solvent casting and annealing, highly oriented and ordered arrays of cylindrical microdomains could be achieved in thin films. By coupling this with the use of a preferential solvent for the minor component, arrays of nanopores in the thin films could easily be achieved with pore diameters down to 15 nm or less. Upon a glancing angle evaporation of a metal onto the surface of the reconstructed film, an etching mask with very high etching contrast could be obtained that allowed the transfer of the pattern produced by the block copolymer into the underlying substrate with exceptional fidelity. All of the processes described were nondisruptive and, as such, can easily be transferred to current microlithographic fabrication processes.

EXPERIMENTAL SECION

Materials. Two poly(styrene-*b*-4-vinylpyridine) (PS-b-P4VP) samples were purchased from Polymer Source and were used without further purification (high molecular weight: M_n,PS = 47.6 kDa, M_n,P4VP = 20.9 kDa, M_w/M_n = 1.14, and low molecular weight: M_n,PS = 25.0 kDa, M_n,P4VP = 7.0 kDa, M_w/M_n = 1.07). PS-b-PVP copolymers were dissolved in toluene/THF solvent mixtures (75/25, v/v) at 70 °C for 2 h and cooled to room temperature to yield a 0.5 wt % polymer solution. Toluene and THF were of analysis grade (Fisher). PS-b-PVP thin films were fabricated by spin coating typically at 2000 rpm and 60 s from a 0.5 wt % toluene/THF solution on the silicon substrate (International Wafer Source, Inc.) cleaned in sulfuric acid and an inorganic oxidizing bath.

Characterization of PS-b-P4VP Thin Films. As-spun films were immersed into small vessel containing ethanol solvent for 20 min to prepare the nanoporous structure. Surface topography of PS-b-P4VP thin films on silicon wafer was imaged using a scanning force microscope (Nanoscope III, Digital Instruments Co.) in tapping mode. For TEM in plain view, the gold evaporated PS-b-P4VP film was floated off from the silicon substrate onto 5 wt % HF solution and colleted on a carbon-coated grid. Bright-field TEM was performed on a (JEOL-1200EX) TEM operating at an accelerating voltage of 100 kV. Grazing incidence small-angle X-ray scattering (GISAXS) measurements were performed on the X22B beamline (National Synchrotron Light Source, Brookhaven National Laboratory) using X-ray with a wavelength of λ = 1.525 Å.

Acknowledgment. This work is supported by the U.S. Department of Energy (DOE), the NSF supported MRSEC and NSEC at the University of Massachusetts Amherst. We thank Prof. E. J. Kramer (UCSB), Prof. R. A. Segalman (UC Berkeley), and Dr. Gial Stein (NIST) for their help and efforts in quantitative characterization of long-range order in 2-D systems. We thank Dr. B. M. Ocko for support of GISAXS measurements at the X22B beamline (National Synchrotron Light Source, Brookhaven National Laboratory, DE-AC02-98CH/0886). We thank Prof. K. L. Wang and M. Ogawa in UCLA for their help of SEM measurement.

Supporting Information Available: Size distribution of cylindrical microdomains, GISAXS pattern, and film thickness information. This material is available free of charge *via* the Internet at http://pubs.acs.org.

REFERENCES AND NOTES

1. Thurn-Albrecht, T.; Schotter, J.; Kästle, G. A.; Emley, N.; Shibauchi, T.; Krusin-Elbaum, L.; Guarini, K.; Black, C. T.; Tuominen, M. T.; Russell, T. P. Ultrahigh-Density Nanowire Arrays Grown in Self-Assembled Diblock Copolymer Templates. *Science* **2000**, *290*, 2126–2129.
2. Fan, H. J.; Werner, P.; Zacharias, M. Semiconductor Nanowires: From Self-Organization to Patterned Growth. *Small* **2006**, *2*, 700–717.
3. Fasolka, M. J.; Mayes, A. M. Block Copolymer Thin Films: Physics and Applications. *Annu. Rev. Mater. Res.* **2001**, *31*, 323–355.
4. Hawker, C. J.; Russell, T. P. Block Copolymer Lithography: Merging "Bottom-Up" with "Top-Down" Processes. *MRS Bulletin* **2005**, *30*, 952–966.
5. Li, M.; Coenjarts, C. A.; Ober, C. K. Patternable Block Copolymers. *Adv. Polym. Sci.* **2005**, *190*, 183–226.
6. Park, M.; Harrison, C.; Chaikin, P. M.; Register, R. A.; Adamson, D. H. Block Copolymer Lithography: Periodic Arrays of $\sim 10^{11}$ Holes in 1 Square Centimeter. *Science* **1997**, *276*, 1401–1404.
7. Thurn-Albrecht, T.; Steiner, R.; DeRouchey, J.; Stafford, C. M.; Huang, E.; Bal, M.; Tuominen, M. T.; Hawker, C. J.; Russell, T. P. Nanoscopic Templates from Oriented Block Copolymer Films. *Adv. Mater.* **2000**, *12*, 787–791.
8. Xu, T.; Stevens, J.; Villa, J.; Goldbach, J. T.; Guarini, K. W.; Black, C. T.; Hawker, C. J.; Russell, T. P. Block Copolymer Surface Reconstruction: A Reversible Route to Nanoporous Films. *Adv. Func. Mater.* **2003**, *13*, 698–702.
9. Kim, G.; Libera, M. Morphological Development in Solvent-Cast Polystyrene-Polybutadiene-Polystyrene (SBS) Triblock Copolymer Thin Films. *Macromolecules* **1998**, *31*, 2569–2577.
10. Kimura, M.; Misner, M. J.; Xu, T.; Kim, S. H.; Russell, T. P. Long-Range Ordering of Diblock Copolymers Induced by Droplet Pinning. *Langmuir* **2003**, *19*, 9910–9913.
11. Ludwigs, S.; Böker, A.; Voronov, A.; Rehse, N.; Magerle, R.; Krausch, G. Self-Assembly of Functional Nanostructures from ABC Triblock Copolymers. *Nat. Mater.* **2003**, *2*, 744–747.
12. Kim, S. H.; Misner, M. J.; Xu, T.; Kimura, M.; Russell, T. P. Highly Oriented and Ordered Arrays from Block Copolymers *via* Solvent Evaporation. *Adv. Mater.* **2004**, *16*, 226–231.
13. Thurn-Albrecht, T.; DeRouchey, J.; Russell, T. P. Overcoming Interfacial Interactions with Electric Fields. *Macromolecules* **2000**, *33*, 3250–3253.

14. Stoykovich, M. P.; Müller, M.; Kim, S. O.; Solak, H. H.; Edwards, E. W.; de Pablo, J. J.; Nealey, P. F. Directed Assembly of Block Copolymer Blends into Nonregular Device-Oriented Structures. *Science* **2005**, *308*, 1442–1446.
15. Kim, S. O.; Solak, H. H.; Stoykovich, M. P.; Ferrier, N. J.; de Pablo, J. J.; Nealey, P. F. Epitaxial Self-Assembly of Block Copolymers on Lithographically Defined Nanopatterned Substrates. *Nature* **2003**, *424*, 411–414.
16. Segalman, R. A.; Yokoyama, H.; Kramer, E. J. Graphoepitaxy of Spherical Domain Block Copolymer Films. *Adv. Mater.* **2001**, *13*, 1152–1155.
17. De Rosa, C.; Park, C.; Thomas, E. L.; Lotz, B. Microdomain Patterns from Directional Eutectic Solidification and Epitaxy. *Nature* **2000**, *405*, 433–437.
18. Mansky, P.; Liu, Y.; Huang, E.; Russell, T. P.; Hawker, C. J. Controlling Polymer-Surface Interactions with Random Copolymer Brushes. *Science* **1997**, *275*, 1458–1460.
19. Drockenmuller, E.; Li, L. Y. T.; Ryu, D. Y.; Harth, E.; Russell, T. P.; Kim, H. C.; Hawker, C. J. Covalent Stabilization of Nanostructures: Robust Block Copolymer Templates from Novel Thermoreactive Systems. *J. Polym. Sci., Part A: Polym. Chem.* **2005**, *43*, 1028–1037.
20. Bodycomb, J.; Funaki, Y.; Kimishima, K.; Hashimoto, T. Single-Grain Lamellar Microdomain from a Diblock Copolymer. *Macromolecules* **1999**, *32*, 2075–2077.
21. Tang, C.; Tracz, A.; Kruk, M.; Zhang, R.; Smilgies, D.-M.; Matyjaszewski, K.; Kowalewski, T. Long-Range Ordered Thin Films of Block Copolymers Prepared by Zone-Casting and Their Thermal Conversion into Ordered Nanostructured Carbon. *J. Am. Chem. Soc.* **2005**, *127*, 6918–6919.
22. Villar, M. A.; Rueda, D. R.; Ania, F.; Thomas, E. L. Study of Oriented Block Copolymers Films Obtained by Roll-Casting. *Polymer* **2002**, *43*, 5139–5145.
23. Hartney, M. A.; Novembre, A. E.; Bates, F. S. Block Copolymers as Bilevel Resists. *J. Vac. Sci. Technol., B.* **1985**, *3*, 1346–1351.
24. Cheng, J. Y.; Ross, C. A.; Thomas, E. L.; Smith, H. I.; Vancso, G. J. Fabrication of Nanostructures with Long-Range Order Using Block Copolymer Lithography. *Appl. Phys. Lett.* **2002**, *81*, 3657–3659.
25. Temple, K.; Kulbaba, K.; Power-Billard, K. N.; Manners, I.; Leach, K. A.; Xu, T.; Russell, T. P.; Hawker, C. J. Spontaneous Vertical Ordering and Pyrolytic Formation of Nanoscopic Ceramic Patterns from Poly(styrene-b-ferrocenylsilane). *Adv. Mater.* **2003**, *15*, 297–300.
26. Cao, L.; Massey, J. A.; Winnik, M. A.; Manners, I.; Riethmuller, S.; Banhart, F.; Spatz, J. P.; Moller, M. *Reactive Ion Etching of Cylindrical Polyferrocenylsilane Block Copolymer Micelles: Fabrication of Ceramic Nanolines on Semiconducting Substrates Adv. Funct. Mater.* **2003**, *13*, 271–276.
27. Lammertink, R. G. H.; Hempenius, M. A.; Van Den Enk, J. E.; Chan, V. Z.-H.; Thomas, E. L.; Vancso, G. J. *Nanostructured Thin Films of Organic-organometallic Block Copolymers: One-step Lithography with Poly(ferrocenylsilanes) by Reactive Ion Etching Adv. Mater.* **2000**, *12*, 98–103.
28. Spatz, J. P.; Herzog, T.; Möbmer, S.; Ziemann, P.; Möller, M. Micellar Inorganic-Polymer Hybrid Systems-A Tool for Nanolithography. *Adv. Mater.* **1999**, *11*, 149–153.
29. Spatz, J. P.; Eibeck, P.; Möbmer, S.; Möller, M.; Herzog, T.; Ziemann, P. Ultrathin Diblock Copolymer/Titanium Laminates-A Tool for Nanolithography. *Adv. Mater.* **1998**, *10*, 849–852.
30. Park, S.; Wang, J.-Y.; Kim, B.; Chen, W.; Russell, T. P. Solvent-Induced Transition from Micelles in Solution to Cylindrical Microdomains in Diblock Copolymer Thin Films. *Macromolecules* **2007**, *40*, 9059–9063.
31. Segalman, R. A.; Hexemer, A.; Hayward, R. C.; Kramer, E. J. Ordering and Melting of Block Copolymer Spherical Domains in 2 and 3 Dimensions. *Macromolecules* **2003**, *36*, 3272–3288.
32. Pashley, D. W.; Menter, J. W.; Basset, G. A. Observation of Dislocation in Metals by Means of Moire Pattern on Electron Micrographs. *Nature (London)* **1957**, *179*, 752–755.
33. Hexemer, A.; Stein, G. E.; Kramer, E. J.; Magonov, S. Block Copolymer Monolayer Structure Measured with Scanning Force Microscopy Moire Patterns. *Macromolecules* **2005**, *38*, 7083–7089.
34. Wu, W.; Cui, B.; Sun, X.-Y.; Zhang, W.; Zhuang, L.; Kong, L.; Chou, S. Y. Large Area High Density Quantized magnetic Disks Fabricated Using Nanoimprint Lithography. *J. Vac. Sci. Technol. B* **1998**, *16*, 3825–3829.
35. We investigated the etching rate of silicon oxide (1.1 nm per sec) by CF_4 reactive ion etching of bare silicon oxide substrate (flow rate: 10 sccm, applied power: 65 W).